NAR Cancer, 2025, **7**, zcaf046
https://doi.org/10.1093/narcan/zcaf046
Cancer Gene Regulation, Chromatin, and Epigenetics

OXFORD

Reversing uL3-mediated chemoresistance through synergistic combination of 5-FU and G-quadruplex ligands

Anna Di Porzio[1,†], Annalisa Pecoraro[1,†], Camilla Danisi[1], Carolina Persico[1], Ludovica D'Auria[2], Marcello Germoglio[1,3], Nunzia Iaccarino[1], Isidoro Feliciello[4,5], Concetta Giancola[1], Antonio Randazzo[1,*], Giulia Russo[1], Annapina Russo[1,*]

[1]Department of Pharmacy, University of Naples Federico II, Via Domenico Montesano 49, 80131 Naples, Italy
[2]CEINGE—Biotecnologie Avanzate Franco Salvatore, Via Gaetano Salvatore 48680131 Naples, Italy
[3]Istituto di Biochimica e Biologia Cellulare, Consiglio Nazionale delle Ricerche, Via Pietro Castellino 111,80131 Naples, Italy
[4]Department of Clinical Medicine and Surgery, University of Naples Federico II, Via Sergio Pansini 5, 80131 Naples,Italy
[5]Department of Molecular Biology, Ruđer Bošković Institute, Bijenička 54, HR-10000 Zagreb, Croatia

*To whom correspondence should be addressed. Email: annapina.russo@unina.it
Correspondence may also be addressed to Antonio Randazzo. Email: antonio.randazzo@unina.it
†The first two authors should be regarded as Joint First Authors.

Abstract

Chemoresistance represents a significant challenge in the chemotherapy of colorectal cancer (CRC), limiting the effectiveness. In this regard, gene expression heterogeneity plays a critical role, influencing cancer cell adaptability and survival under chemotherapy. Our previous data revealed that ribosomal protein uL3 positively correlates with both chemoresistance and poor prognosis in CRC patients. This study explores the combination of 5-fluorouracil (5-FU), the first-line treatment of CRC, with G-quadruplex (G4) ligands, which have recently emerged as promising candidates for cancer therapy, to overcome uL3-mediated chemoresistance. We found that resistant p53-deficient and uL3-silenced CRC cells showed increased levels of G4 structures compared to both sensitive p53-deficient and p53-proficient cells, thereby exhibiting vulnerability to the cytotoxic effects of two well-established G4 ligands, pyridostatin (PDS) and RHPS4. The combination of 5-FU with PDS or RHPS4 exhibited a synergistic effect, selectively targeting tumor cells. This approach enabled a >10-fold reduction in the 5-FU dose, improving treatment efficacy. The effectiveness of this combination was further validated *in vivo* using uL3-silenced CRC cell-derived xenografts in a chicken embryo model. Overall, our findings highlight a novel and promising combination strategy that targets chemoresistance in CRCs characterized by non-functional p53 and reduced levels of uL3.

Graphical abstract

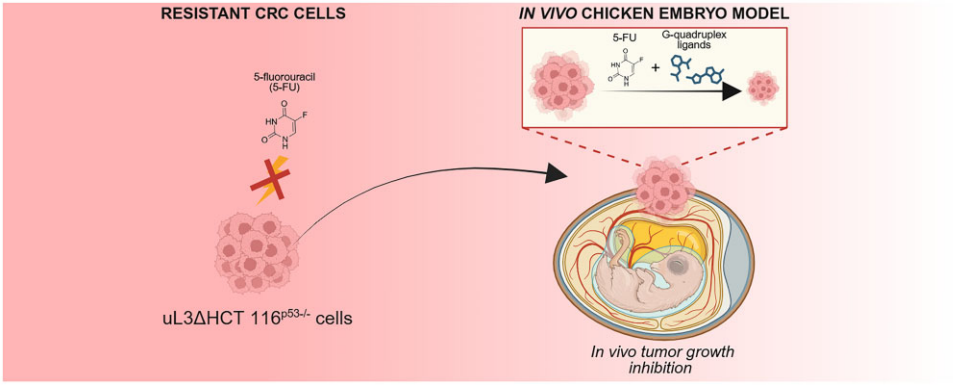

Introduction

Cancer recurrence and metastasis are the primary cause of colorectal cancer (CRC)-related death [1]. From the perspective of therapeutic response, CRC is a very heterogeneous disease [2], and the genetic profiles of the tumor determine the prognosis and response to the treatment [3, 4]. Many clinical studies demonstrated the prognostic relevance of the tumor suppressor protein p53 for many human tumor types including CRC [5, 6]. The p53 protein plays a critical role in activating anti-proliferative/pro-apoptotic pathways and facilitating

Received: June 18, 2025. **Revised:** September 25, 2025. **Accepted:** October 15, 2025

the effects of antitumor agents [7, 8]. Loss of p53 function from mutation, which occurs in ∼60% of CRCs [9], leads to drug resistance, resulting in poor response of tumors to a wide range of clinical treatment regimens [10]. Consequently, targeted therapies based on the knowledge of the specific molecular characteristics of p53-deficient CRCs are essential for developing more effective treatment strategies and determining the optimal dosages to achieve successful tumor treatment. In this context, our previous results provided data indicating that the ribosomal protein uL3 (formerly rpL3) is a crucial player conferring multidrug resistance to CRC cells lacking functional p53 [11–14]. In addition, more recently, transcriptome analysis of a large cohort of CRC patients unveiled a strict correlation between uL3 expression and CRC patients' outcomes. Specifically, the reduced uL3 levels were associated with a poor response to therapeutic treatment. These studies have identified uL3 as an important player in response to chemotherapeutic drugs, suggesting a possible application of uL3 as a predictive biomarker of treatment response in p53-deficient CRC [15]. We have previously produced a cellular model of p53-deleted CRC cell line stably silenced of uL3 [11], showing resistance to the most common chemotherapeutic drugs, and extensively detailed the molecular mechanisms underlying chemoresistance [16]. In the absence of p53, loss of uL3 associates with alteration of the epithelial-mesenchymal transition (EMT) program, increased cell migration and invasion, induction of autophagy, and inhibition of apoptosis [13, 17]. *In vivo* experiments using the chicken chorioallantoic membrane (CAM) model demonstrated that p53-deficient and uL3-silenced CRC cells show a more aggressive cancer phenotype, displaying more vascularization and a higher propensity to form metastasis spreading to the liver and lungs [18]. 5-Fluorouracil (5-FU) remains the first-line treatment for CRC, but response to the treatment, overall survival, and associated toxicity are influenced by inter-individual variations, posing a critical hurdle in cancer management and adversely impacting patients' quality of life [19, 20].

Over the past decades, noncanonical DNA secondary structures have emerged as promising targets for cancer therapy [21]. Among these alternative structural arrangements, G-quadruplexes (G4s)—four-stranded helical conformations that can form in guanine-rich DNA regions—stand out as the most extensively studied ones [22, 23]. Interestingly, it has been shown that sequences capable of folding into G4 structures are predominantly located at biologically relevant nuclear genomic sites, such as telomeres and oncogene promoters [24, 25], as well as within the mitochondrial DNA [26, 27], suggesting that these structures could offer exciting therapeutic opportunities [23, 28]. In this regard, multiple studies have shown that ligand-induced G4 stabilization can potentially result in remarkable antitumor effects [29–32]. As a result, cancer research has intensively directed its efforts toward the development of compounds capable of stabilizing endogenous G4 structures [33–42].

Recent findings have confirmed that G4s are implicated in the transcription of genes involved in differentiation, cancer progression, and metabolic regulation [43, 44]. The variation in G4 content is a crucial factor in differentiating between normal and tumor cells, as increased G4 formation may be a characteristic of some cancers [45, 46].

Herein, to identify a novel promising treatment option for CRCs lacking functional p53 and expressing low levels of uL3 that are resistant to common chemotherapeutic drugs, we focused on approaches based on G4 ligands, which have previously been shown to be able to sensitize cancer cells to standard chemotherapies [47, 48]. Particularly, we investigated the potential of combining 5-FU with two well-known G4 binders, pyridostatin (PDS) and RHPS4, to overcome uL3-mediated chemoresistance and potentially reduce the doses and side effects of 5-FU.

In this study, we demonstrate that (i) the G4 structure content was increased in resistant uL3-silenced CRC cells (uL3ΔHCT 116$^{p53-/-}$) at both nuclear and mitochondrial genome levels; (ii) resistant uL3-silenced CRC cells showed sensitivity to G4 binders PDS and RHPS4; (iii) simultaneous treatment with 5-FU and PDS or RHPS4 showed a selective, synergistic effect in resistant uL3ΔHCT 116$^{p53-/-}$ cells, resensitizing them to 5-FU; and (iv) xenografts derived from resistant uL3ΔHCT 116$^{p53-/-}$ cells exposed to 5-FU, combined with PDS or RHPS4, exhibited a significant reduction in tumor weight and volume, validating the proposed therapeutic strategy *in vivo*.

Overall, our study demonstrates that the proposed therapeutic strategy, combining 5-FU with G4 ligands (PDS or RHPS4), exhibits cytotoxic efficacy at low doses of 5-FU, selective action on cancer cells, and anticancer effectiveness *in vivo*, making it a promising candidate for the treatment of p53-deficient CRCs with low uL3 levels.

Materials and methods

Materials

Dulbecco's modified Eagle's medium (DMEM), Dulbecco's phosphate buffered saline (PBS), fetal bovine serum (FBS), penicillin, streptomycin, and cell culture plasticware were provided by Euroclone S.p.A. (Milan, Italy). Matrigel® was purchased from Corning® (Corning, NY, USA). L-glutamine was purchased from Thermo Fisher Scientific (Waltham, MA, USA). Dimethyl sulfoxide (DMSO), 4% paraformaldehyde, Triton X-100, and bovine serum albumin (BSA) were supplied by HiMedia (Pennsylvania, USA). Tween 20, the Hoechst 33258 solution, Mowiol 4-88, 5-FU, and RHPS4 were purchased from Merck (St. Louis, MO, USA), whereas PDS was provided by Aurogene S.r.l. (Rome, Italy). 3-(4,5-Dimethylthiazol-2-yl)-2,5-diphenyltetrazolium bromide (MTT) was purchased from Merck KGaA (Darmstadt, Germany).

The following antibodies were used for the immunofluorescence experiments: recombinant 6× His/3× FLAG-tagged BG4 antibody; rabbit anti-FLAG antibody (Cell Signaling Technology, #2368S); mouse anti-Tom20 antibody (F-10) (Santa Cruz Biotechnology, #17764); donkey anti-rabbit IgG (H + L) highly cross-adsorbed secondary antibody (Alexa Fluor 488 Conjugate) (Thermo Fisher Scientific, #A-21206); and goat anti-mouse IgG (H + L) highly cross-adsorbed secondary antibody (Alexa Fluor 647 Conjugate) (Thermo Fisher Scientific, #A-21235).

Expression and purification of BG4 single chain antibody

Recombinant 6× His/3× FLAG-tagged BG4 was produced in *Escherichia coli* using pSANG10-3F-BG4 (Addgene, #55756) as follows: BL21 (DE3) competent cells were transformed with pSANG10-3F plasmid expressing BG4 scFv anti-G4 antibody. The transformed cells were inoculated in 2× TY

medium [1.6% (w:v) bacto tryptone, 1% (w:v) bacto yeast extract, 0.5% (w:v) NaCl] containing 2% (w:v) glucose and 50 μg/ml kanamycin for 16 h at 30°C. Then, the overnight cell culture was inoculated in autoinduction medium [1% (w:v) bacto peptone, 0.5% (w:v) bacto yeast extract] containing 25 mM KH_2PO_4, 50 mM NH_4Cl, 5 mM Na_2SO_4, 2 mM $MgSO_4$, 10 μM $FeCl_3$, 2 μM $MnCl_2$, 4 μM $CaCl_2$, 2 μM $ZnSO_4$, 0.4 μM $CoCl_2$, 0.4 μM $CuCl_2$, 0.4 μM $NiCl_2$, 0.4 μM Na_2MoO_4, 0.4 μM H_3BO_3, 0.05% (w:v) glucose, 0.2% (w:v) lactose, 0.5% (w:v) glycerol, and 50 μg/ml kanamycin for 6 h at 30°C and overnight at 22°C. Bacterial cells were centrifuged for 30 min at 4000 × *g* (4°C). Cell pellet was lysed in TES buffer [50 mM Tris–HCl, 1 mM EDTA (ethylenediaminetetraacetic acid), 20% sucrose] on ice and stirred in the presence of EDTA-free protease inhibitor cocktail (cOmplete tablets Roche) for 5 min at 4°C. The cell extract was diluted 1:1 with 1:5 TES buffer (10 mM Tris–HCl, 0.2 mM EDTA, 4% sucrose) containing 2 mM $MgSO_4$ and Benzonase (12.5 units/ml) and gently stirred for 30 min at 4°C, prior to centrifugation for 20 min at 8000 × *g* (4°C). The supernatant was filtered (0.45 μm), and the antibody was purified using HisPur™ Cobalt Superflow Agarose resin (Thermo Fisher Scientific) pre-equilibrated in PBS containing 20 mM imidazole. Supernatant and resin were mixed in a glass beaker with magnetic bar for 30 min at 4°C, then transferred into a chromatography column. The resin was washed twice with 3-column volume PBS supplemented with 100 mM NaCl and 10 mM imidazole. The BG4 antibody was eluted with PBS 1× supplemented with 250 mM imidazole (pH 8.0). The elution buffer was exchanged with inner cell salt buffer [25 mM HEPES–NaOH (pH 7.6), 110 mM KCl, 10.5 mM NaCl, 1 mM $MgCl_2$]. The eluted fractions containing the BG4 antibody were pooled, and the sample concentrated using an Amicon Ultra-15 Centrifugal Filter Unit with a 10-kDa cutoff (Millipore). Protein concentration and quality were checked by sodium dodecyl sulfate–polyacrylamide gel electrophoresis (Supplementary Fig. S1A). Next, the enzyme-linked immunosorbent assay was performed similar to those described previously [49] to ensure that the BG4 preparation has high affinity and specificity for G4 structures (Supplementary Fig. S1B).

Cell culture and treatments

CRC cell lines (HCT 116$^{p53+/+}$, HCT 116$^{p53-/-}$, and uL3ΔHCT 116$^{p53-/-}$, a cell line derived from HCT 116$^{p53-/-}$ cells and stably silenced of uL3) were cultured in DMEM and supplemented with 10% FBS, 2 mM L-glutamine, and 50 U/ml penicillin–streptomycin under a humidified atmosphere of 5% CO_2 at 37°C. Normal human colon mucosal epithelial cell line (NCM460D) was purchased from CEINGE Biotecnologie Avanzate—Franco Salvatore Cell Culture Facility and grown in DMEM supplemented with 10% FBS, 2 mM L-glutamine, and 50 U/ml penicillin–streptomycin. Cells were subcultured at 90% confluence every 3 days and maintained at 37°C in a humidified atmosphere containing 5% CO_2.

The G4 binders used in this study (PDS and RHPS4) were dissolved in 100% DMSO to prepare stock solutions at 80 mM concentration, whereas 5-FU was dissolved in 100% DMSO at 100 mM. Prior to use, each compound was diluted in cell culture medium to the desired concentration.

Drug treatments were performed by exposing cells to varying concentrations of 5-FU, PDS, and RHPS4, either individually or in combination (5-FU + PDS and 5-FU + RHPS4), for 48 h. Treatments were refreshed after 24 h.

G-quadruplexes (G4s) and mitochondria immunofluorescence co-staining

CRC cells were seeded on sterile coverslips, in a 24-well plate, at a density of 100 000 cells/well (HCT 116$^{p53+/+}$ and HCT 116$^{p53-/-}$) or 60 000 cells/well (uL3ΔHCT 116$^{p53-/-}$) and maintained at 37°C. The following day, cells were washed with PBS, fixed in 4% paraformaldehyde [10 min, room temperature (RT)], and then permeabilized with PBS containing 0.1% Triton-X (10 min, RT). Blocking of nonspecific binding sites was achieved by incubation with 0.5% FBS in PBST (PBS + 0.1% Tween 20) at 37°C for 1 h. Afterward, cells were incubated with the BG4 antibody (1:250, 1 h, 37°C), rinsed three times with PBS, and then co-incubated with both the rabbit anti-FLAG (1:800) and mouse anti-Tom20 antibodies (1:100) at 37°C for 1 h. After three more rinsing steps with PBS, cells were co-stained with the Alexa Fluor 488 anti-rabbit IgG and the Alexa Fluor 647 anti-mouse IgG (1:500, for 1 h, RT). Nuclei were counterstained with the Hoechst 33258 solution (1:3000, 10 min, RT). Finally, coverslips were rinsed once with distilled water and mounted on microscope slides using Mowiol 4-88.

For image acquisition, z-stacks of three planes were obtained using a confocal microscope (Zeiss LSM 980) equipped with a Plan-Apochromat 63×/1.4 NA oil immersion objective. The acquired z-stacks were processed to generate maximum intensity projections. Subsequently, G4 foci and mitochondria were segmented, and their quantities and co-localization were quantified using the Image Analysis module of ZEISS ZEN Blue 3.1 software.

Cell viability assay

HCT 116$^{p53+/+}$, HCT 116$^{p53-/-}$, uL3ΔHCT 116$^{p53-/-}$ cells, and NCM460D (10×10^3 cells/well) were plated in serum-containing media in 96-well plates and incubated for 24 h at 37°C. For the simultaneous treatments, cells were treated with increasing concentrations of 5-FU and G4 ligand (PDS or RHPS4). After 24 h, the culture medium was removed, and cells were exposed to fresh drug solutions for an additional 24 h. Sequential treatments were performed exposing cells to increasing concentrations of 5-FU for 24 h, followed by 24 h of treatment with the G4 ligand, or vice versa. The 48 h cytotoxicity profiles of PDS, RHPS4, and 5-FU alone, on CRC cell lines, were also delineated. At the end of the treatments, cell viability was assessed by adding MTT, as previously reported [50]. The absorbance value of the solution in each well was detected at 570 nm using a Biotek Synergy H1 Hybrid multiplate reader. All MTT experiments were performed in triplicate. Cell viability was expressed as the percentage of absorbance values in treated samples with respect to that of the control (100%). The concentration of compound able to reduce by 50% the cellular viability (IC_{50}) was calculated by means of a nonlinear regression analysis using Prism 10.2.1 (GraphPad, San Diego, CA, USA).

Analysis of drug–drug interaction

The IC_{50} value of each drug, alone or in combination, was used to calculate the corresponding combination index (CI) according to the Chou–Talalay method [51]. Particularly, for

a two-drug combination, the model can be written as follows:

$$\mathrm{CI} = \frac{D1}{Dx1} + \frac{D2}{Dx2}, \quad (1)$$

where $D1$ is the IC_{50} of Drug 1 in the combination, $Dx1$ is the IC_{50} of Drug 1 alone, $D2$ is the IC_{50} of Drug 2 in the combination, and $Dx2$ is the IC_{50} of Drug 2 alone. Overall, CI values <0.90 denoted synergism, CI values >1.10 indicated antagonism and CI values in the range 0.90–1.10 implied an additive effect.

The dose-reduction index (DRI) for each drug in a synergistic combination was also calculated to assess the magnitude of dose reduction allowed, compared to each drug alone:

$$\mathrm{DRI} = \frac{Dx}{D}, \quad (2)$$

which is a simple inversion of Equation 1.

DRI values below 1 indicated unfavorable dose reduction, values above 1 denoted favorable dose reduction, and values equal to 1 implied no dose reduction for each combined drug.

Tumor chicken chorioallantoic membrane (TCAM) model

The tumor chicken chorioallantoic membrane (TCAM) model was performed on fertilized chicken eggs, which were incubated as previously described [52]. The first day of incubation was considered as egg development day (EDD) zero (EDD0). On EDD4, the eggs were opened: first, a small hole was punched into the eggshell at the "bottom" of the egg; then, around 3 ml of albumen was removed using a syringe, and the hole was closed with adhesive tape; subsequently, a window was cut on the top side of the egg using sharp scissors; and finally, the window was closed with an additional strip of tape to prevent drying out and contaminating the CAM. The opened eggs were further kept in a stationary incubator. On EDD9, 20 µl of the suspension of uL3ΔHCT 116$^{p53-/-}$ cells (3×10^6 cells) in serum-free medium mixed with 20 µl of Matrigel was applied close to the allantoid vein bifurcation using a pipette while avoiding direct contact with the CAM. After xenografting, the eggs were left standing upright for 5–10 min in order to allow the cells to settle and then sealed with adhesive tape. The eggs were subsequently placed back in the incubator and kept until EDD17. During this period, frequent inspections through the window in the eggshell were performed to evaluate tumor growth and to confirm that the chicken embryos were still alive. Tumor sizes were measured by excising and recording their wet weight on EDD17. The tumor volume was measured with a digital caliper and calculated using the ellipsoid formula (length × width × height × 0.52) in mm^3. Statistical comparisons were made as previously described [53]. In the European Union countries, experimentation with chicken embryos is allowed and does not require ethical approval from animal experimentation committees on the condition that experiments begin and end before hatching (Directive 2010/63/EU).

Results and discussion

G-quadruplex (G4) content in sensitive and resistant CRC cells

To explore the potential of G4 ligands in overcoming uL3-mediated chemoresistance, we first assessed the content of G4 structures in sensitive and resistant CRC cells, at both nuclear and mitochondrial (mt) genome levels, using immunofluorescence microscopy. Specifically, we employed the BG4 antibody, which specifically recognizes G4 structures [49], and the anti-Tom20 antibody, a mitochondrial marker, to process sensitive p53-proficient (HCT 116$^{p53+/+}$) and p53-deficient (HCT 116$^{p53-/-}$) CRC cells, as well as resistant p53-deleted CRC cells stably silenced of uL3 (uL3ΔHCT 116$^{p53-/-}$) [11].

At the nuclear genome level, the G4 content of resistant uL3ΔHCT 116$^{p53-/-}$ cells was ∼40% higher than that observed in both HCT 116$^{p53-/-}$ and HCT 116$^{p53+/+}$ cells (Fig. 1A and B). Moreover, we found that the absence of p53 resulted in an increase in mt G4 structures, with HCT 116$^{p53-/-}$ cells exhibiting nearly twice the number of mt G4s compared to HCT 116$^{p53+/+}$ cells (Fig. 1A and C). Of note, the mt DNA of resistant uL3ΔHCT 116$^{p53-/-}$ cells exhibited the highest levels of G4s among the tested cell lines (Fig. 1A and C). This result was further validated by colocalization area analysis between the G4 foci and mitochondria, which revealed a significant increase of mt G4 content in resistant CRC cells (Fig. 1A, D and E).

These findings suggest an involvement of G4 structures in sustaining uL3-related drug resistance and metastatic phenotype. The increased G4 levels could induce chromatin remodeling and contribute to transcriptional programs supporting uL3ΔHCT 116$^{p53-/-}$ cell survival under therapeutic stress. This hypothesis aligns with recent findings showing that G4 enrichment correlates with enhanced transcription of signaling pathways known to promote drug resistance [54], including genes involved in EMT and WNT signalling as observed in uL3ΔHCT 116$^{p53-/-}$ [17].

Moreover, ribosomal protein depletion, including uL3 loss, is known to cause ribosomal stress [17] that can trigger chromatin remodeling through histone modifications and altered nucleosome positioning [55]. These changes may increase the accessibility of G-rich genomic regions, favoring their folding into G4 structures. Ribosomal stress has been shown to affect mitochondrial homeostasis, leading to dysregulation of mitochondrial transcription, reactive oxygen species (ROS) accumulation, and activation of nuclear stress pathways that influence DNA secondary structure formation [56]. In line with this, our previous studies demonstrated that the loss of uL3 caused ribosomal stress and mitochondrial dysfunction, resulting in ROS accumulation [17, 18]. We have also observed that the loss of uL3 alters the transcriptome of HCT 116$^{p53-/-}$ [17], including changes in the expression of helicases and other G4-resolving enzymes. Since these enzymes are crucial for maintaining G4 homeostasis, their dysfunction may lead to an imbalance between G4 formation and resolution, favoring G4 accumulation and genome instability [57].

Overall, these results pointed G4 regulatory network as a potential target in p53-deficient CRC cells, prompting us to explore therapeutic strategies involving G4 ligands.

Analysis of dose–response curves for single treatments with PDS, RHPS4 and 5-FU in sensitive and resistant CRC cells

The increased abundance of G4 structures observed in resistant p53-deficient and uL3-silenced CRC cells prompted us to investigate whether these cells might be vulnerable to G4-targeting ligands. Specifically, given the elevated content of G4s both in the nucleus and mitochondria, we chose to test ligands that could target these two distinct compartments.

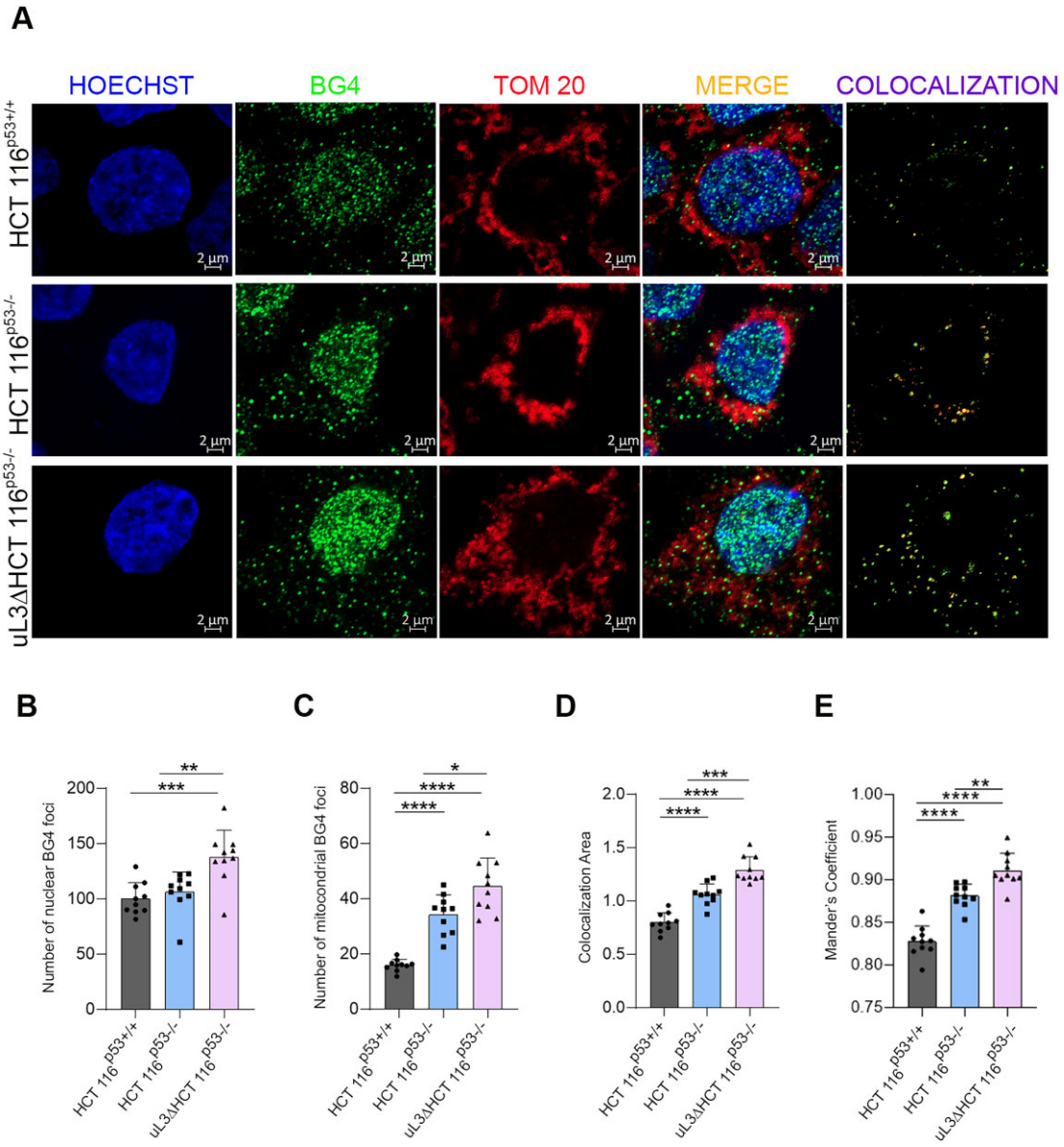

Figure 1. G4 foci content in sensitive and resistant CRC cells. (**A**) Representative immunofluorescence images showing G4 foci in HCT 116$^{p53+/+}$, HCT 116$^{p53-/-}$, and uL3ΔHCT 116$^{p53-/-}$ cells. Nuclei were stained with the Hoechst solution (blue), mitochondria with the anti-Tom20 antibody (red), and G4 structures with BG4 (green). The merged channels are reported. In addition, the colocalized red and green signal spots are also reported to show the localization of G4 foci in mitochondria. Scale bar: 2 μm. (**B**) Quantitative analysis of nuclear G4 foci. (**C**) Quantitative analysis of mitochondrial G4 foci. (**D**) Quantification showing colocalization area of BG4 with Tom20 signal. All analyses were performed by employing the Image Analysis package of ZEISS ZEN Blue 3.1 software. An average of 350 cells were screened for each cell line. Histograms show the mean ± SD of two independent experiments. (**E**) Colocalization between BG4 and Tom20 signals was also quantified using Mander's coefficient, analyzing an average of 300 cells for each cell line. The statistical significance was calculated by one-way ANOVA test on GraphPad Prism 10.2.1 (∗$P < .05$; ∗∗$P < .01$; ∗∗∗$P < .001$; and ∗∗∗∗$P < .0001$). Refer also to Supplementary Fig. S2.

Therefore, among the well-characterized G4-stabilizing compounds, we focused our attention on PDS, known to preferentially stabilize nuclear G4 structures and induce DNA double-strand breaks [23, 58], and RHPS4, which has been shown to predominantly localize to mitochondria in noncancerous mouse embryonic fibroblasts, disrupting mitochondrial replication and transcription [27, 59, 60].

We assessed the cytotoxic effects of both PDS and RHPS4 on sensitive HCT 116$^{p53+/+}$ and HCT 116$^{p53-/-}$ cells, as well as on resistant uL3ΔHCT 116$^{p53-/-}$ cells, using MTT assays to determine their respective IC_{50} values. As shown in Fig. 2A and B, both compounds reduced cell viability in a dose-dependent manner, with increasing concentrations leading to progressively greater reductions in cell survival. Notably, the cytotoxic activity of the two G4 ligands was comparable between p53-proficient and p53-deficient CRC cells, yielding IC_{50} values of 8.68 μM versus 8.55 μM for PDS and 7.44 μM versus 6.89 μM for RHPS4, respectively. These results indicate that p53 status does not substantially affect the cellular response to these G4 ligands.

Importantly, the resistant uL3ΔHCT 116$^{p53-/-}$ cells also exhibited sensitivity to both PDS (IC_{50} = 8.25 μM) and RHPS4 (IC_{50} = 9.49 μM), confirming their susceptibility to G4-targeting compounds.

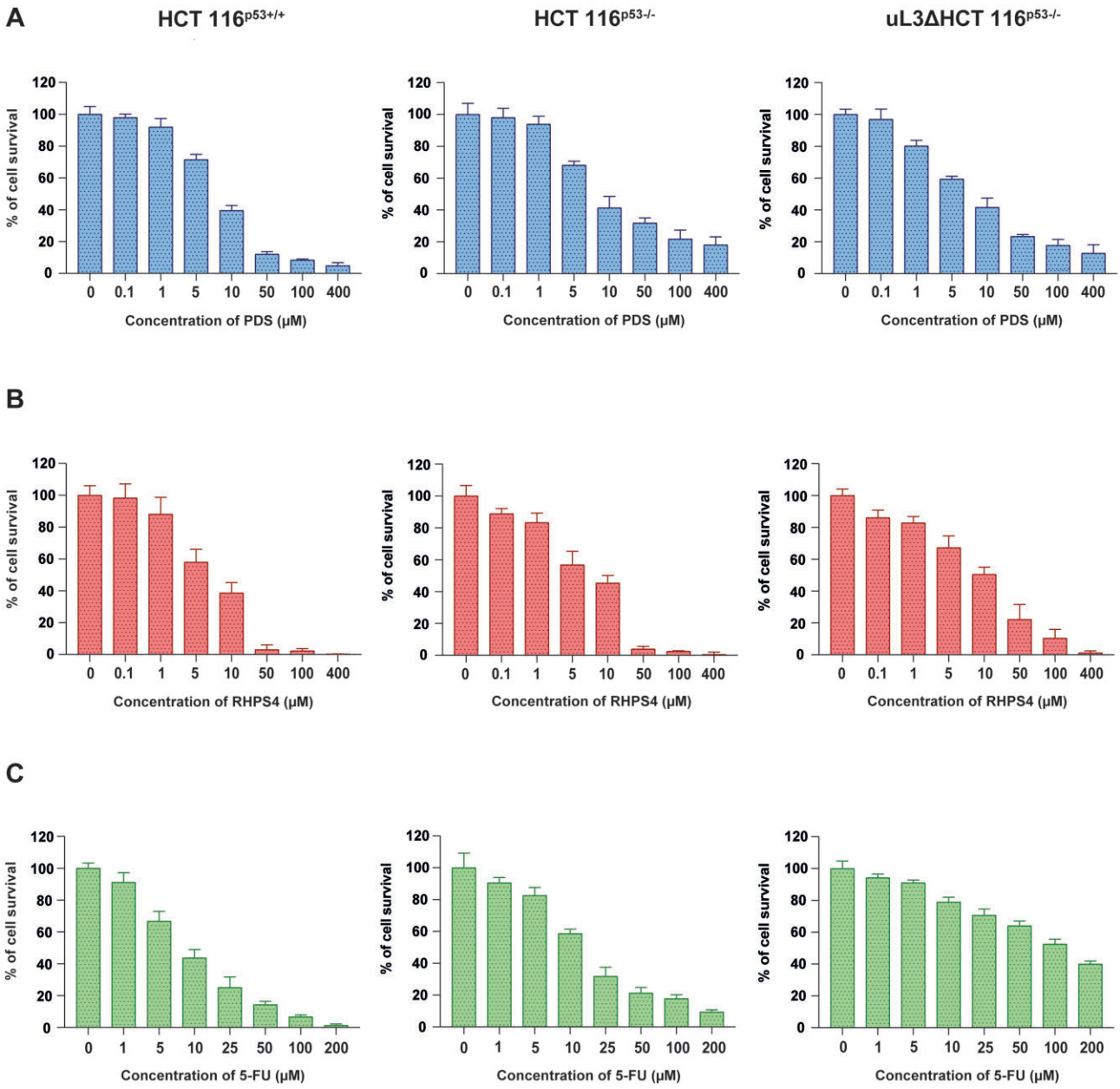

Figure 2. Cytotoxic effect of (**A**) PDS, (**B**) RHPS4, and (**C**) 5-FU in HCT 116$^{p53+/+}$, HCT 116$^{p53-/-}$, and uL3ΔHCT 116$^{p53-/-}$ cells. Cells were treated with increasing concentrations of the indicated drug for 48 h. Cell viability was assessed using the MTT assay. The graphs show the mean ± SD of three independent experiments.

In parallel, we evaluated the cytotoxic response to 5-FU, the first-line chemotherapeutic agent for CRC, across the same cell lines. As shown in Fig. 2C, 5-FU exerted dose-dependent cytotoxic effects on both p53-proficient and p53-deficient CRC cells. However, consistent with previous findings, p53 status significantly influenced drug sensitivity: HCT 116$^{p53+/+}$ cells were nearly twice as sensitive to 5-FU (IC_{50} = 8.82 μM) as HCT 116$^{p53-/-}$ cells (IC_{50} = 15.14 μM). In contrast, uL3 silencing drastically reduced 5-FU efficacy in uL3ΔHCT 116$^{p53-/-}$ cells (IC_{50} = 127.90 μM), clearly indicating resistance to the treatment and corroborating our earlier results (Fig. 2C) [11, 61].

It is known that p53 deficiency and loss of ribosomal proteins, including uL3, promote ribosomal stress and impair DNA damage checkpoint control [17, 62, 63]. These processes may sensitize cells to G4-induced DNA secondary structures and replication blocks. Thus, although our findings indicate that both G4 ligands have p53-independent activity, the simultaneous uL3 loss and p53 dysfunction may act in concert to destabilize transcriptional and replication programs, further exacerbating G4-associated stress.

The observed susceptibility of resistant uL3ΔHCT 116$^{p53-/-}$ cells to G4 ligands raises important considerations regarding the potential applicability of these molecules to treat resistant CRCs.

Cytotoxic effect of combined treatments with 5-FU plus G4 ligands

Next, to investigate whether combining 5-FU with G4 ligands could help overcome chemoresistance in CRC cells, we carried out *in vitro* MTT assays by exposing HCT 116$^{p53+/+}$, HCT

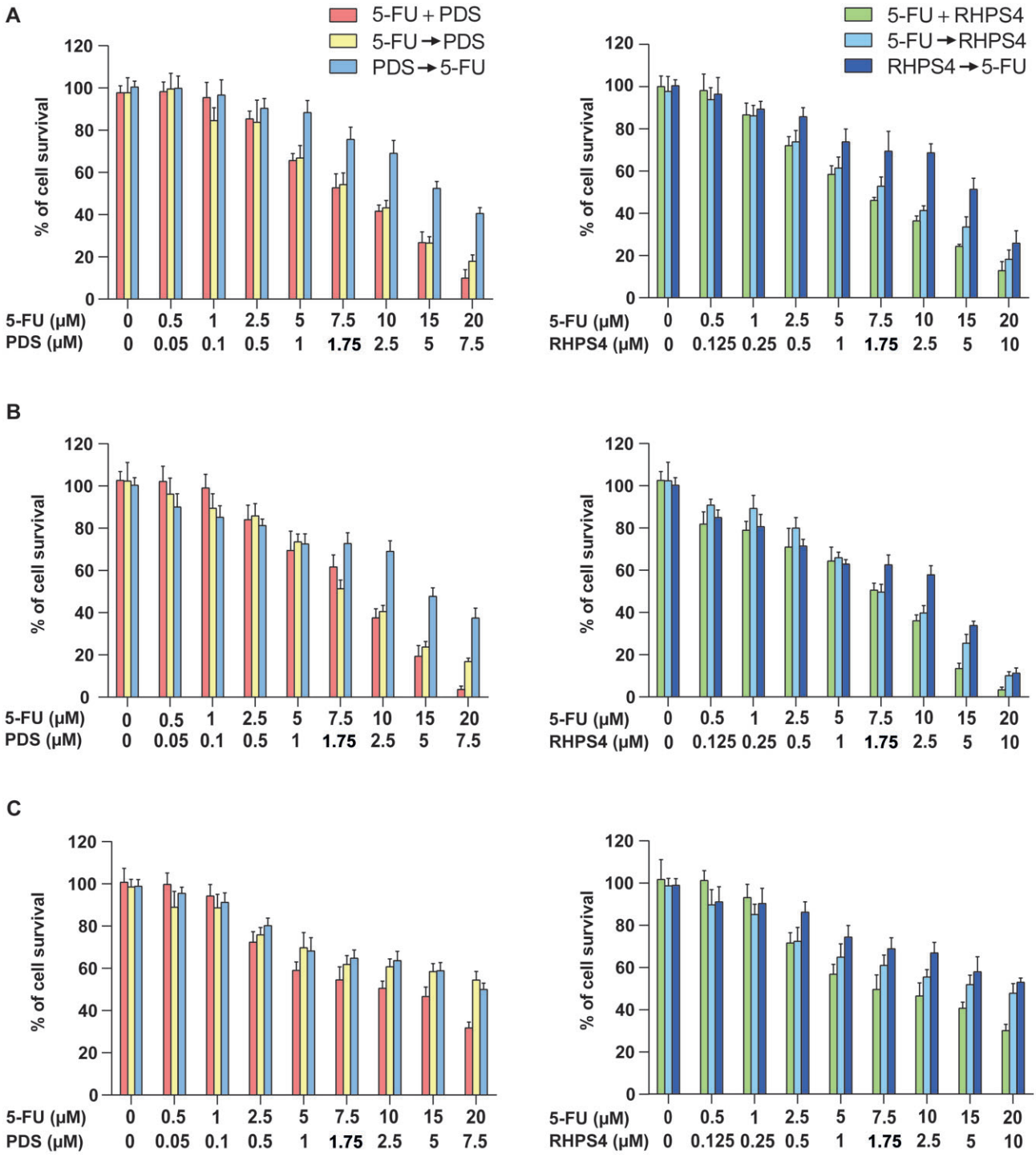

Figure 3. Cytotoxic effect of simultaneous and sequential treatments with increasing concentrations of 5-FU + PDS or 5-FU + RHPS4 on (**A**) HCT $116^{p53+/+}$, (**B**) HCT $116^{p53-/-}$, and (**C**) uL3ΔHCT $116^{p53-/-}$ cells. Simultaneous treatments were performed for 48 h, administering to cells the indicated concentration of the two drugs concurrently. In sequential treatments, cells were exposed to the first drug for 24 h, followed by another 24 h of treatment with the second drug. The graphs show the mean ± SD of three independent experiments.

$116^{p53-/-}$, and uL3ΔHCT $116^{p53-/-}$ cells to 5-FU, either in simultaneous or sequential combination with PDS or RHPS4. Particularly, to better assess the impact of these combinations, we used lower concentrations of each molecule compared to those in Fig. 2. Specifically, the concentrations used were 0.5–20 μM for 5-FU, 0.05–7.5 μM for PDS, and 0.125–10 μM for RHPS4. In simultaneous combination treatments, cells were exposed to both drugs for 48 h. In sequential treatments, cells were first pretreated with a single drug for 24 h, followed by exposure to a second drug for another 24 h, maintaining a total treatment duration of 48 h (Fig. 3). At the end of the treatments, the Chou–Talalay method was employed to calculate the CIs from our MTT experiments, enabling a quantitative assessment of the interactions between the combined agents [64].

According to our results, the simultaneous treatment of HCT $116^{p53+/+}$ cells with 5-FU + PDS resulted in a nearly additive effect (CI = 1.10 ± 0.12), meaning that the cytotoxic ef-

Table 1. Combination index (CI) values obtained from the 48 h simultaneous treatments with 5-FU and PDS on HCT 116$^{p53+/+}$, HCT 116$^{p53-/-}$, and uL3ΔHCT 116 $^{p53-/-}$ cells

Cell line	IC_{50} value (μM)			CI value[a]	Effect
	5-FU	PDS	Combination		
HCT 116$^{p53+/+}$	8.82 ± 0.31	8.68 ± 0.25	5-FU: 7.70 ± 0.14 PDS: 1.83 ± 0.04	1.10 ± 0.12	Additive
HCT 116$^{p53-/-}$	15.14 ± 2.55	8.55 ± 0.92	5-FU: 7.92 ± 0.27 PDS: 1.90 ± 0.04	0.75 ± 0.09	Moderate synergism
uL3ΔHCT 116$^{p53-/-}$	127.90 ± 9.05	8.25 ± 1.82	5-FU: 10.02 ± 0.59 PDS: 2.72 ± 0.22	0.41 ± 0.15	Synergism

[a]CI values were calculated with the Chou–Talalay method (see Equation 1 in the "Materials and methods" section). Data are presented as mean ± SD of three independent experiments.
The IC_{50} of the individual and combined drugs are also reported.

Table 2. Combination index (CI) values obtained from the 48 h simultaneous treatments with 5-FU and RHPS4 on HCT 116$^{p53+/+}$, HCT 116$^{p53-/-}$, and uL3ΔHCT 116$^{p53-/-}$ cells

Cell line	IC_{50} value (μM)			CI value[a]	Effect
	5-FU	RHPS4	Combination		
HCT 116$^{p53+/+}$	8.82 ± 0.31	7.44 ± 0.83	5-FU: 6.07 ± 0.61 RHPS4: 1.49 ± 0.16	0.89 ± 0.09	Slight synergism
HCT 116$^{p53-/-}$	15.14 ± 2.55	6.89 ± 2.64	5-FU: 5.60 ± 0.89 RHPS4: 1.33 ± 0.15	0.59 ± 0.23	Synergism
uL3ΔHCT 116$^{p53-/-}$	127.90 ± 9.05	9.49 ± 1.85	5-FU: 8.21 ± 0.98 RHPS4: 3.09 ± 0.78	0.39 ± 0.02	Synergism

[a]CI values were calculated with the Chou–Talalay method (see Equation 1 in the "Materials and methods" section). Data are presented as mean ± SD of three independent experiments.
The IC_{50} of the individual and combined drugs are also reported.

fect of the drug association proved to be basically equal to the mathematical sum of the effects of the drugs when given alone (Table 1). By contrast, upon 5-FU + RHPS4 treatment, a slight synergism could be observed (CI = 0.89 ± 0.09) (Table 2). In HCT 116$^{p53-/-}$ cells, both 5-FU + PDS and 5-FU + RHPS4 simultaneous treatments led to interesting synergistic effects, even though of varying magnitude (CI values of 0.75 ± 0.09 and 0.59 ± 0.23, respectively). Strikingly, the strongest synergism between 5-FU and G4 ligands was found in resistant uL3ΔHCT 116$^{p53-/-}$ cells, providing CI values of 0.41 ± 0.15 and 0.39 ± 0.02 for the 5-FU + PDS and 5-FU + RHPS4 simultaneous combinations, respectively (Tables 1 and 2). These findings demonstrate that G4 binders could effectively resensitize resistant uL3ΔHCT 116$^{p53-/-}$ cells to the chemotherapeutic agent 5-FU.

As shown in Fig. 3, simultaneous treatments proved to be generally more cytotoxic than sequential ones, highlighting the strong dependence of drug efficacy on the treatment schedule employed. Also, the specific order of drug administration in sequential treatments significantly affected the cytotoxic outcomes, especially on sensitive HCT 116$^{p53+/+}$ and HCT 116$^{p53-/-}$ cells, possibly due to the distinct mechanisms of action of the tested anticancer agents. Indeed, the treatment with 5-FU followed by the G4 ligand (5-FU → G4 ligand) was demonstrated to be more effective than the reverse drug sequence administration, which resulted in lower cytotoxic effects. One possible explanation is that cellular stress induced by 5-FU may promote the formation of G4 structures [65–67], which are subsequently recognized and stabilized by the G4 ligand.

Furthermore, to assess the extent to which the dose of the drugs in combination could be reduced due to the observed synergistic effects, DRI values were also calculated for all synergistic simultaneous combinations (Tables 3 and 4). DRI values less than, greater than, or equal to 1 denoted unfavorable, favorable, and no dose reduction for each combined drug, respectively. Importantly, under the experimental conditions used, all DRI values exceeded 1 for both combination of 5-FU and the G4 ligands. Particularly, the DRI values of 5-FU

Table 3. Dose-reduction index (DRI) values obtained from the 48 h simultaneous treatments of HCT 116$^{p53+/+}$, HCT 116$^{p53-/-}$, and uL3ΔHCT 116$^{p53-/-}$ cells with 5-FU and PDS

Cell line	DRI value[a]	
	5-FU	PDS
HCT 116$^{p53+/+}$	–	–
HCT 116$^{p53-/-}$	1.91 ± 0.26	4.50 ± 0.38
uL3ΔHCT 116$^{p53-/-}$	13.31 ± 1.16	3.30 ± 1.39

[a]DRI values were obtained using Equation 2 (see the "Materials and methods" section) only for the synergistic combinations. Values are reported as mean ± SD of three independent experiments.

Table 4. Dose-reduction index (DRI) values obtained from the 48 h simultaneous treatments of HCT 116 $^{p53+/+}$, HCT 116$^{p53-/-}$ and uL3ΔHCT 116$^{p53-/-}$ cells with 5-FU and RHPS4

Cell line	DRI value[a]	
	5-FU	RHPS4
HCT 116$^{p53+/+}$	1.46 ± 0.20	4.99 ± 0.04
HCT 116$^{p53-/-}$	2.77 ± 0.90	5.34 ± 2.59
uL3ΔHCT 116$^{p53-/-}$	15.62 ± 0.75	3.10 ± 0.19

[a]DRI values were obtained using Equation 2 (see the "Materials and methods" section). Values are reported as mean ± SD of three independent experiments.

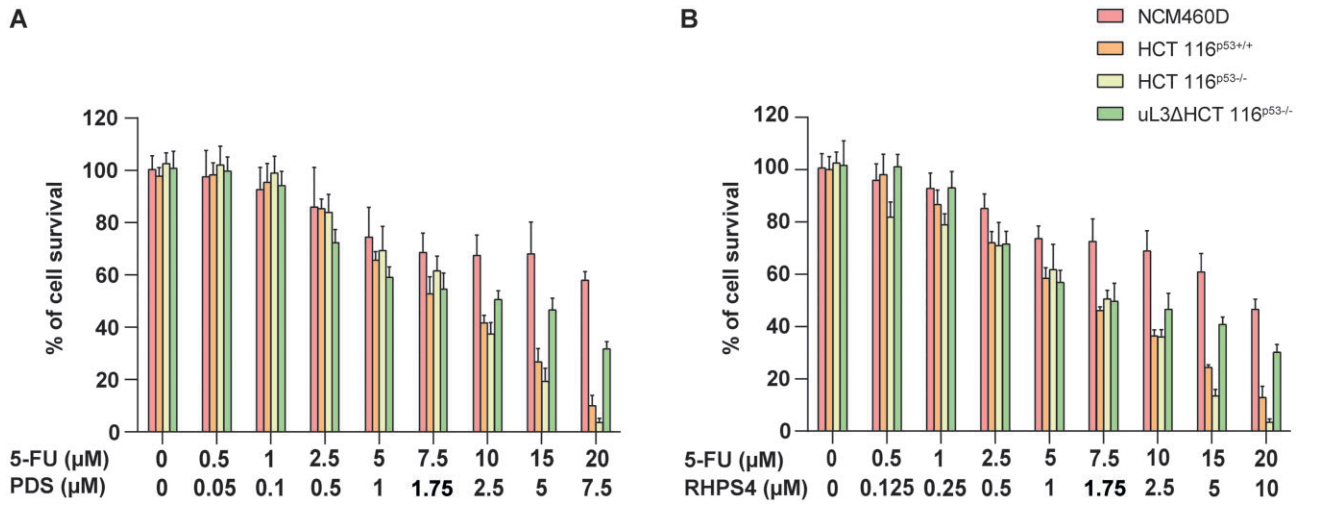

Figure 4. Cytotoxicity profiles of the simultaneous treatments with increasing concentrations of (**A**) 5-FU + PDS and (**B**) 5-FU + RHPS4 on nontumorigenic NCM460D, HCT 116$^{p53+/+}$, HCT 116$^{p53-/-}$, and uL3ΔHCT 116$^{p53-/-}$ cells. Combined treatments were performed for 48 h, administering to cells the indicated concentration of the two drugs concurrently. The graphs show the mean ± SD of three independent experiments.

in combination with either PDS or RHPS4, in resistant uL3-silenced CRC cells, proved to be notably high (13.31 ± 1.16 and 15.62 ± 0.75, respectively), indicating that such combined treatments could allow for a >10-fold reduction in the required 5-FU dose.

Overall, when 5-FU and G4 ligands were coadministered to CRC cells for 48 h, synergistic cytotoxic effects were observed in nearly all cases. Notably, the most pronounced synergy was observed in resistant uL3ΔHCT 116$^{p53-/-}$ cells, where the lowest CIs and the highest DRI values for 5-FU were recorded (Tables 1–4). Additionally, the extent of cytotoxicity induced by the combined treatments was found to be highly dependent on both the treatment schedule (simultaneous or sequential) and the sequence of drug administration employed (G4 ligand → 5-FU or 5-FU → G4 ligand), with the simultaneous treatment schedule generally demonstrating to be the most effective approach (Fig. 3).

Combined treatments with 5-FU and G4 ligands in nontumorigenic colon cells

A major limitation of most chemotherapeutic regimens is their lack of specificity in selectively targeting cancer cells [68]. To evaluate the therapeutic potential of the combinations under investigation, their cytotoxicity was also assessed in normal human colon mucosal epithelial cells (NCM460D) using the same treatment schedule and concentration ranges applied to CRC cells (HCT 116$^{p53+/+}$, HCT 116$^{p53-/-}$, and uL3ΔHCT 116$^{p53-/-}$).

Strikingly, as shown in Fig. 4, both 5-FU + PDS and 5-FU + RHPS4 combinations exhibited lower toxicity in NCM460D cells compared to CRC cells across nearly all tested concentrations. In particular, treatment with 5-FU and PDS (Fig. 4A) reduced NCM460D cell viability in a dose-dependent manner; however, cell survival remained above 50% even at the highest concentration (20 μM 5-FU plus 7.5 μM PDS). Similarly, treatment with 5-FU and RHPS4 (Fig. 4B) led to a gradual decrease in viability, yet survival dropped below 50% only at the highest concentration tested (20 μM 5-FU plus 10 μM RHPS4). By contrast, at this concentration, viability was reduced to ∼10%, 5%, and 30% in HCT 116$^{p53+/+}$, HCT 116$^{p53-/-}$, and uL3ΔHCT 116$^{p53-/-}$ cells, respectively. Importantly, due to the limited cytotoxicity of the combined treatments toward normal colon cells, it was not possible to calculate the corresponding IC_{50} values.

Collectively, these findings highlight the remarkable tumor selectivity of the tested drug combinations *in vitro*, supporting their strong potential for therapeutic application.

In vivo antitumor effect of combined treatments with 5-FU and G4 ligands in TCAM model

To evaluate the chemotherapeutic efficacy of the proposed combined treatments in preclinical models, we established uL3ΔHCT 116$^{p53-/-}$ cell line-derived xenografts on the chicken embryo CAM [18]. Specifically, fertilized eggs were incubated for 4 days, when a hole was made in the shell. After 5 days, uL3ΔHCT 116$^{p53-/-}$ cells were transplanted onto the CAM. Then, the eggs were incubated for 6 additional days to allow formation of a distinct tumor mass. Every day, visual inspection was used to track the formation of tumors and the vitality of chicken embryos. On EDD15 and EDD16, topical administration of PDS or RHPS4 (2.5 μM), alone or in combination with 5-FU (10 μM), was performed on the xenografts (Fig. 5A). On EDD17, CAM xenografts were harvested, weighed, and measured using a digital caliper (Fig. 5B-C).

A significant reduction in the growth of treated xenografts was observed. Specifically, xenografts treated with either PDS or RHPS4 alone showed significantly lower tumor weight and volume compared with untreated tumors (Fig. 5C and D). Of note, xenografts exposed to the simultaneous treatment with either 5-FU + PDS or 5-FU + RHPS4 showed a further reduction in tumor weight and volume compared to untreated or PDS-/RHPS4-treated tumors (Fig. 5C and D). These data provide evidence for the efficacy of the proposed combined treatments, also in a preclinical model.

Altogether, our results indicate that the G4 ligands, PDS and RHPS4, combined with 5-FU are promising candidates for targeting p53-deficient tumors and for overcoming uL3-mediated chemoresistance *in vivo*, thus highlighting their potential for further clinical development.

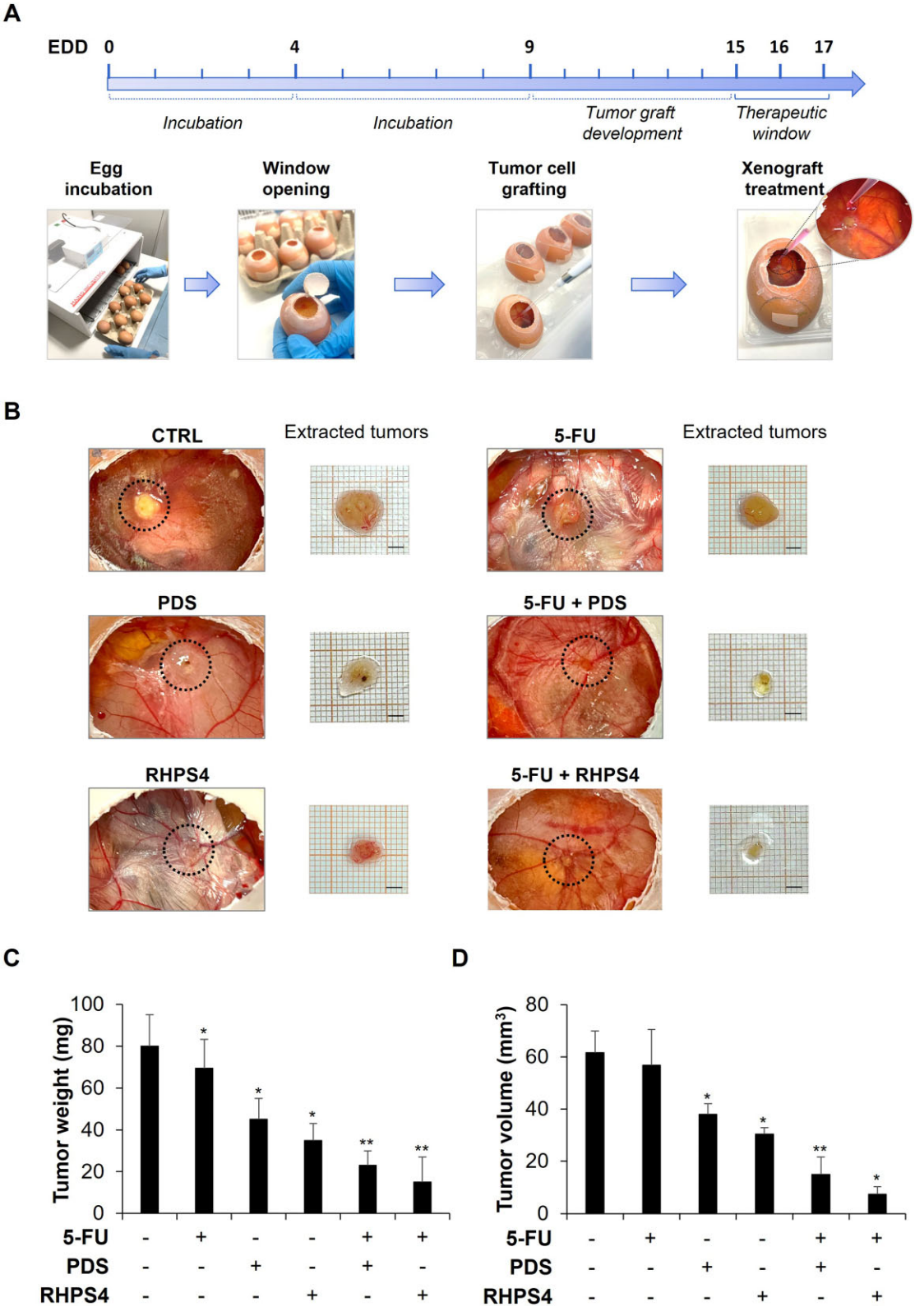

Figure 5. Antitumor effects of PDS or RHPS4, alone or in combination with 5-FU, in TCAM model. (**A**) Schematic representation of general workflow for generating uL3ΔHCT 116$^{p53-/-}$cell line-derived xenografts onto the CAM of developing chicken embryos. In brief, chicken embryos ($n = 50$) were incubated at 37.5°C and 55% humidity upon arrival and until day 4 post-fertilization. At EDD4, a small window was opened on each eggshell. The eggs were then incubated until EDD9, when uL3ΔHCT 116$^{p53-/-}$ cells were engrafted onto CAM surface. The xenografts ($n = 8$) received topical treatments by directly pipetting the dissolved drugs (2.5 μM of PDS or RHPS4, either alone or in combination with 10 μM of 5-FU) on EDD15 and EDD16, keeping the overall treatment duration of 48 h. At EDD17, embryos were sacrificed, and tumors were harvested to evaluate the potential antitumor effects of test substances. (**B**) Macroscopic images of uL3ΔHCT 116$^{p53-/-}$ cell line-derived tumors were captured on EDD17. Selected areas of CAM in which uL3ΔHCT 116$^{p53-/-}$cells were engrafted are shown. Scale bar: 3 mm. (**C, D**) On EDD17, excised tumors were weighed and measured using a digital caliper to determine the effect of the treatments on tumor growth. Data were analyzed using a two-way ANOVA test. $*P < .05$ and $**P < .01$ versus untreated cell-derived tumors.

Conclusions

Chemoresistance remains a major obstacle in the treatment of CRC, critically undermining the efficacy of standard chemotherapeutic agents. Previous studies have identified the ribosomal protein uL3 as a key driver of resistance, particularly in the context of p53 deficiency.

In this study, we demonstrate the potential of G4 ligands, specifically PDS and RHPS4, to overcome uL3-mediated chemoresistance in p53-deficient CRC cells. Notably, these ligands effectively resensitized resistant CRC cells to 5-FU, enabling a dramatic reduction, over 10-fold, in the required drug dosage. Among the various treatment regimens tested, the simultaneous administration of 5-FU and G4 ligands produced the strongest effects, inducing robust synergistic cytotoxicity *in vitro*.

Crucially, this combinatorial strategy also translated into a significant suppression of tumor growth in an *in vivo* chicken embryo xenograft model, further supporting its potential clinical applicability. However, given the limitations of this system, these findings remain to be validated using murine xenograft models for the translation to human doses. Furthermore, we cannot exclude that PDS and RHPS4 may exert additional off-target effects that could impact the clinical translation of the proposed treatments.

Overall, our findings position G4-targeting compounds as promising therapeutic tools for counteracting chemoresistance in p53-deficient CRC. By restoring sensitivity to 5-FU and allowing for dose reduction, this approach offers a dual benefit: enhancing treatment efficacy while potentially reducing adverse effects. These results open new avenues for the development of targeted therapies in CRC patients with p53 deficiency and uL3 dysregulation, molecular features frequently associated with poor prognosis and limited treatment options.

Acknowledgements

Microscopy experiments were done at the CEINGE Advanced Light Microscopy Facility.

The graphical abstract was created in BioRender [Russo, A. (2025); https://BioRender.com/warr8q0].

Author contributions: Anna Di Porzio (Investigation, Methodology, Validation, Data curation, Writing—original draft), Annalisa Pecoraro (Investigation, Methodology, Validation, Data curation, Writing—original draft), Camilla Danisi (Investigation, Metodology, Validation), Carolina Persico (Investigation, Metodology, Validation), Ludovica D'Auria (Metodology, Validation), Marcello Germoglio (Metodology, Validation), Nunzia Iaccarino (Investigation, Metodology, Data curation, Validation), Isidoro Feliciello (Metodology, Resources), Concetta Giancola (Metodology, Resources), Antonio Randazzo (Conceptualization, Supervision, Writing—review & editing, Project administration, Funding acquisition), Giulia Russo (Supervision, Review & editing), and Annapina Russo (Conceptualization, Supervision, Writing—review & editing, Project administration, Funding acquisition).

Supplementary data

Supplementary data is available at NAR Cancer online.

Conflict of interest

None declared.

Funding

This research was funded by PNRR-Missione 4 Componente 2 Investimento 1.4 "Poten- ziamento strutture di ricerca e creazione di "campioni nazionali di R&S" su alcune Key Enabling Technologies" Centro Nazionale "National Center for Gene Therapy and Drugs based on RNA Technology" Codice progetto MUR: CN00000041–CUP UNINA: E63C22000940007 Progetto finanziato dall'Unione Europea-NextGenerationEU (to Annapina Russo, A.R., C.G.)

This work was also supported by the Italian Association for Cancer Research (AIRC) (IG #26313 to A.R. and IG #23198 to C.G.).

Data availability

The data underlying this article are available in the article.

References

1. Rumpold H, Niedersüß-Beke D, Heiler C *et al.* Prediction of mortality in metastatic colorectal cancer in a real-life population: a multicenter explorative analysis. *BMC Cancer* 2020;20:1149. https://doi.org/10.1186/s12885-020-07656-w
2. Rachiglio AM, Sacco A, Forgione L *et al.* Colorectal cancer genomic biomarkers in the clinical management of patients with metastatic colorectal carcinoma. *Explor Target Antitumor Ther* 2020;1:53–70. https://doi.org/10.37349/etat.2020.00004
3. Fanelli GN, Dal Pozzo CA, Depetris I *et al.* The heterogeneous clinical and pathological landscapes of metastatic *Braf*-mutated colorectal cancer. *Cancer Cell Int* 2020;20:30. https://doi.org/10.1186/s12935-020-1117-2
4. Nguyen HT, Duong H-Q. The molecular characteristics of colorectal cancer: implications for diagnosis and therapy. *Oncol Lett* 2018;16:9–18.
5. Kim KM, Ahn A-R, Park HS *et al.* Clinical significance of p53 protein expression and TP53 variation status in colorectal cancer. *BMC Cancer* 2022;22:940. https://doi.org/10.1186/s12885-022-10039-y
6. Wang H, Guo M, Wei H *et al.* Targeting p53 pathways: mechanisms, structures and advances in therapy. *Sig Transduct Target Ther* 2023;8:92. https://doi.org/10.1038/s41392-023-01347-1
7. Aubrey BJ, Kelly GL, Janic A *et al.* How does p53 induce apoptosis and how does this relate to p53-mediated tumour suppression? *Cell Death Differ* 2018;25:104–13. https://doi.org/10.1038/cdd.2017.169
8. Merlino F, Pecoraro A, Longobardi G *et al.* Development and nanoparticle-mediated delivery of novel MDM2/MDM4 heterodimer peptide inhibitors to enhance 5-fluorouracil nucleolar stress in colorectal cancer cells. *J Med Chem* 2024;67:1812–24. https://doi.org/10.1021/acs.jmedchem.3c01312
9. Marei HE, Althani A, Afifi N *et al.* p53 signaling in cancer progression and therapy. *Cancer Cell Int* 2021;21:703. https://doi.org/10.1186/s12935-021-02396-8
10. Li W, Li L, Yang H *et al.* Unraveling the role of *TP53* in colorectal cancer therapy: from wild-type regulation to mutant. *Front Biosci (Landmark Ed)* 2024;29:272. https://doi.org/10.31083/j.fbl2907272
11. Pagliara V, Saide A, Mitidieri E *et al.* 5-FU targets rpL3 to induce mitochondrial apoptosis via cystathionine-β-synthase in colon cancer cells lacking p53. *Oncotarget* 2016;7:50333–48. https://doi.org/10.18632/oncotarget.10385

12. Esposito D, Crescenzi E, Sagar V *et al.* Human rpL3 plays a crucial role in cell response to nucleolar stress induced by 5-FU and L-OHP. *Oncotarget* 2014;5:11737–51. https://doi.org/10.18632/oncotarget.2591
13. Pecoraro A, Carotenuto P, Russo G *et al.* Ribosomal protein uL3 targets E2F1 and Cyclin D1 in cancer cell response to nucleolar stress. *Sci Rep* 2019;9:15431. https://doi.org/10.1038/s41598-019-51723-7
14. Mosca L, Pagano M, Borzacchiello L *et al.* S-Adenosylmethionine increases the sensitivity of human colorectal cancer cells to 5-Fluorouracil by inhibiting P-glycoprotein expression and NF-κB activation. *Int J Mol Sci* 2021;22:9286. https://doi.org/10.3390/ijms22179286
15. Carotenuto P, Pecoraro A, Brignola C *et al.* Combining β-carotene with 5-FU via polymeric nanoparticles as a novel therapeutic strategy to overcome uL3-mediated chemoresistance in p53-deleted colorectal cancer cells. *Mol Pharm* 2023;20:2326–40. https://doi.org/10.1021/acs.molpharmaceut.2c00876
16. Russo A, Saide A, Cagliani R *et al.* rpL3 promotes the apoptosis of p53 mutated lung cancer cells by down-regulating CBS and NFκB upon 5-FU treatment. *Sci Rep* 2016;6:38369. https://doi.org/10.1038/srep38369
17. Pecoraro A, Carotenuto P, Franco B *et al.* Role of uL3 in the crosstalk between nucleolar stress and autophagy in colon cancer cells. *Int J Mol Sci* 2020;21:2143. https://doi.org/10.3390/ijms21062143
18. Brignola C, Pecoraro A, Danisi C *et al.* uL3 regulates redox metabolism and ferroptosis sensitivity of p53-deleted colorectal cancer cells. *Antioxidants* 2024;13:757. https://doi.org/10.3390/antiox13070757
19. Pardini B, Bermejo JL, Naccarati A *et al.* Inherited variability in a master regulator polymorphism (rs4846126) associates with survival in 5-FU treated colorectal cancer patients. *Mut Res* 2014;766-767:7–13. https://doi.org/10.1016/j.mrfmmm.2014.05.007
20. Gmeiner WH, Okechukwu CC. Review of 5-FU resistance mechanisms in colorectal cancer: clinical significance of attenuated on-target effects. *Cancer Drug Resist* 2023;6:257–72. https://doi.org/10.20517/cdr.2022.136
21. Kosiol N, Juranek S, Brossart P *et al.* G-quadruplexes: a promising target for cancer therapy. *Mol Cancer* 2021;20:40. https://doi.org/10.1186/s12943-021-01328-4
22. Huppert JL. Structure, location and interactions of G-quadruplexes. *FEBS J* 2010;277:3452–8. https://doi.org/10.1111/j.1742-4658.2010.07758.x
23. Spiegel J, Adhikari S, Balasubramanian S. The structure and function of DNA G-quadruplexes. *Trends Chem* 2020;2:123–36. https://doi.org/10.1016/j.trechm.2019.07.002
24. Marsico G, Chambers VS, Sahakyan AB *et al.* Whole genome experimental maps of DNA G-quadruplexes in multiple species. *Nucleic Acids Res* 2019;47:3862–74. https://doi.org/10.1093/nar/gkz179
25. Romano F, Di Porzio A, Iaccarino N *et al.* G-quadruplexes in cancer-related gene promoters: from identification to therapeutic targeting. *Expert Opin Ther Pat* 2023;33:745–73. https://doi.org/10.1080/13543776.2023.2271168
26. Falabella M, Fernandez RJ, Johnson FB *et al.* Potential roles for G-quadruplexes in mitochondria. *Curr Med Chem* 2019;26:2918–32. https://doi.org/10.2174/0929867325666180228165527
27. Sahayasheela VJ, Yu Z, Hidaka T *et al.* Mitochondria and G-quadruplex evolution: an intertwined relationship. *Trends Genet* 2023;39:15–30. https://doi.org/10.1016/j.tig.2022.10.006
28. Rhodes D, Lipps HJ. G-quadruplexes and their regulatory roles in biology. *Nucleic Acids Res* 2015;43:8627–37. https://doi.org/10.1093/nar/gkv862
29. Salvati E, Leonetti C, Rizzo A *et al.* Telomere damage induced by the G-quadruplex ligand RHPS4 has an antitumor effect. *J Clin Invest* 2007;117:3236–47. https://doi.org/10.1172/JCI32461
30. Amato J, Pagano A, Capasso D *et al.* Targeting the BCL2 gene promoter G-quadruplex with a new class of furopyridazinone-based molecules. *ChemMedChem* 2018;13:406–10. https://doi.org/10.1002/cmdc.201700749
31. Zegers J, Peters M, Albada B. DNA G-quadruplex-stabilizing metal complexes as anticancer drugs. *J Biol Inorg Chem* 2023;28:117–38. https://doi.org/10.1007/s00775-022-01973-0
32. Holden L, Curley RC, Avella G *et al.* Targeting mitochondrial guanine quadruplexes for photoactivatable chemotherapy in hypoxic environments. *Angew Chem Int Ed Engl* 2024;63:e202408581. https://doi.org/10.1002/anie.202408581
33. Pagano B, Cosconati S, Gabelica V *et al.* State-of-the-art methodologies for the discovery and characterization of DNA G-quadruplex binders. *Curr Pharm Des* 2012;18:1880–99. https://doi.org/10.2174/138161212799958332
34. Pagano A, Iaccarino N, Abdelhamid MAS *et al.* Common G-quadruplex binding agents found to interact with i-motif-forming DNA: unexpected multi-target-directed compounds. *Front Chem* 2018;6:281. https://doi.org/10.3389/fchem.2018.00281
35. Pagano B, Iaccarino N, Di Porzio A *et al.* Screening of DNA G-quadruplex stabilizing ligands by nano differential scanning fluorimetry. *Analyst* 2019;144:6512–6. https://doi.org/10.1039/C9AN01463B
36. Di Porzio A, Galli U, Amato J *et al.* Synthesis and characterization of bis-triazolyl-pyridine derivatives as noncanonical DNA-interacting compounds. *Int J Mol Sci* 2021;22:11959. https://doi.org/10.3390/ijms222111959
37. Marzano S, Pagano B, Iaccarino N *et al.* Targeting of telomeric repeat-containing RNA G-quadruplexes: from screening to biophysical and biological characterization of a new hit compound. *Int J Mol Sci* 2021;22:10315. https://doi.org/10.3390/ijms221910315
38. Moraca F, Marzano S, D'Amico F *et al.* Ligand-based drug repurposing strategy identified SARS-CoV-2 RNA G-quadruplex binders. *Chem Commun* 2022;58:11913–6. https://doi.org/10.1039/D2CC03135C
39. Nocentini A, Di Porzio A, Bonardi A *et al.* Development of a multi-targeted chemotherapeutic approach based on G-quadruplex stabilisation and carbonic anhydrase inhibition. *J Enzyme Inhib Med Chem* 2024;39:2366236. https://doi.org/10.1080/14756366.2024.2366236
40. Figueiredo J, Mergny J-L, Cruz C. G-quadruplex ligands in cancer therapy: progress, challenges, and clinical perspectives. *Life Sci* 2024;340:122481. https://doi.org/10.1016/j.lfs.2024.122481
41. Moraca F, Arciuolo V, Marzano S *et al.* Repurposing FDA-approved drugs to target G-quadruplexes in breast cancer. *Eur J Med Chem* 2025;285:117245. https://doi.org/10.1016/j.ejmech.2025.117245
42. Piccolo M, Russo C, Arciuolo V *et al.* Design, synthesis, and anticancer activity of drug-like iron chelators/G-quadruplex binders as synergic dual targeting agents. *J Med Chem* 2025;68:1245–59. https://doi.org/10.1021/acs.jmedchem.4c01665
43. Marzano S, Pinto G, Di Porzio A *et al.* Identifying G-quadruplex-interacting proteins in cancer-related gene promoters. *Commun Chem* 2025;8:64. https://doi.org/10.1038/s42004-025-01462-w
44. Lin J, Gong Z, Lu Y *et al.* Recent progress and potential of G4 ligands in cancer immunotherapy. *Molecules* 2025;30:1805.
45. Biffi G, Tannahill D, Miller J *et al.* Elevated levels of G-quadruplex formation in human stomach and liver cancer tissues. *PLoS One* 2014;9:e102711. https://doi.org/10.1371/journal.pone.0102711
46. Zhang H, Zhou J, Ye Y. Prediction and validation of circulating G-quadruplexes as a novel biomarker in colorectal cancer. *J Gastrointest Oncol* 2024;15:286–98. https://doi.org/10.21037/jgo-24-26
47. Persico C, Iaccarino N, Romano F *et al.* Sensitization of melanoma cells to standard chemotherapy: G-quadruplex binders as

synergistic agents. *NAR Cancer* 2024;6:zcae042. https://doi.org/10.1093/narcan/zcae042
48. Iachettini S, Biroccio A, Zizza P. Therapeutic use of G4-ligands in cancer: state-of-the-art and future perspectives. *Pharmaceuticals* 2024;17:771. https://doi.org/10.3390/ph17060771
49. Biffi G, Tannahill D, McCafferty J *et al.* Quantitative visualization of DNA G-quadruplex structures in human cells. *Nature Chem* 2013;5:182–6. https://doi.org/10.1038/nchem.1548
50. Virgilio A, Benigno D, Pecoraro A *et al.* Exploring new potential anticancer activities of the G-quadruplexes formed by [(GTG2T(G3T)3] and its derivatives with an abasic site replacing single thymidine. *Int J Mol Sci* 2021;22:7040. https://doi.org/10.3390/ijms22137040
51. Chou T-C. Drug combination studies and their synergy quantification using the Chou–Talalay method. *Cancer Res* 2010;70:440–6. https://doi.org/10.1158/0008-5472.CAN-09-1947
52. Bellavita R, Pecoraro A, Palladino S *et al.* Transport across membrane meets biophysics to unveil the mechanism of action of a novel gH625 analogue. *Eur J Pharm Sci* 2025;212:107204.
53. De Filippis D, Russo A, De Stefano D *et al.* Palmitoylethanolamide inhibits rMCP-5 expression by regulating MITF activation in rat chronic granulomatous inflammation. *Eur J Pharmacol* 2014;725:64–9. https://doi.org/10.1016/j.ejphar.2013.12.021
54. Robinson J, Flint G, Garner I *et al.* G-quadruplex structures regulate long-range transcriptional reprogramming to promote drug resistance in ovarian cancer cells. *Genome Biol* 2025;26:183. https://doi.org/10.1186/s13059-025-03654-y
55. Chen Y, Liang R, Li Y *et al.* Chromatin accessibility: biological functions, molecular mechanisms and therapeutic application. *Sig Transduct Target Ther* 2024;9:340. https://doi.org/10.1038/s41392-024-02030-9
56. Xu X, Pang Y, Fan X. Mitochondria in oxidative stress, inflammation and aging: from mechanisms to therapeutic advances. *Sig Transduct Target Ther* 2025;10:190. https://doi.org/10.1038/s41392-025-02253-4
57. Pavlova AV, Kubareva EA, Monakhova MV *et al.* Impact of G-quadruplexes on the regulation of genome integrity, DNA damage and repair. *Biomolecules* 2021;11:1284. https://doi.org/10.3390/biom11091284
58. Rodriguez R, Müller S, Yeoman JA *et al.* A novel small molecule that alters shelterin integrity and triggers a DNA-damage response at telomeres. *J Am Chem Soc* 2008;130:15758–9. https://doi.org/10.1021/ja805615w
59. Falabella M, Kolesar JE, Wallace C *et al.* G-quadruplex dynamics contribute to regulation of mitochondrial gene expression. *Sci Rep* 2019;9:5605. https://doi.org/10.1038/s41598-019-41464-y
60. Doimo M, Chaudhari N, Abrahamsson S *et al.* Enhanced mitochondrial G-quadruplex formation impedes replication fork progression leading to mtDNA loss in human cells. *Nucleic Acids Res* 2023;51:7392–408. https://doi.org/10.1093/nar/gkad535
61. Russo A, Maiolino S, Pagliara V *et al.* Enhancement of 5-FU sensitivity by the proapoptotic rpL3 gene in p53 null colon cancer cells through combined polymer nanoparticles. *Oncotarget* 2016;7:79670–87. https://doi.org/10.18632/oncotarget.13216
62. Lindström MS, Bartek J, Maya-Mendoza A. p53 at the crossroad of DNA replication and ribosome biogenesis stress pathways. *Cell Death Differ* 2022;29:972–82. https://doi.org/10.1038/s41418-022-00999-w
63. Pecoraro A, Virgilio A, Esposito V *et al.* uL3 mediated nucleolar stress pathway as a new mechanism of action of antiproliferative G-quadruplex TBA derivatives in colon cancer cells. *Biomolecules* 2020;10:583. https://doi.org/10.3390/biom10040583
64. Chou TC, Talalay P. Quantitative analysis of dose-effect relationships: the combined effects of multiple drugs or enzyme inhibitors. *Adv Enzyme Regul* 1984;22:27–55. https://doi.org/10.1016/0065-2571(84)90007-4
65. Byrd AK, Zybailov BL, Maddukuri L *et al.* Evidence that G-quadruplex DNA accumulates in the cytoplasm and participates in stress granule assembly in response to oxidative stress. *J Biol Chem* 2016;291:18041–57. https://doi.org/10.1074/jbc.M116.718478
66. Fleming AM, Burrows CJ. Oxidative stress-mediated epigenetic regulation by G-quadruplexes. *NAR Cancer* 2021;3:zcab038. https://doi.org/10.1093/narcan/zcab038
67. Kharel P, Fay M, Manasova EV *et al.* Stress promotes RNA G-quadruplex folding in human cells. *Nat Commun* 2023;14:205. https://doi.org/10.1038/s41467-023-35811-x
68. Anand U, Dey A, Chandel AKS *et al.* Cancer chemotherapy and beyond: current status, drug candidates, associated risks and progress in targeted therapeutics. *Genes Dis* 2022;10:1367–401. https://doi.org/10.1016/j.gendis.2022.02.007

Received: June 18, 2025. **Revised:** September 25, 2025. **Accepted:** October 15, 2025